

A WAVELET GALERKIN METHOD EMPLOYING B-SPLINE BASES FOR SOLID MECHANICS PROBLEMS WITHOUT THE USE OF A FICTITIOUS DOMAIN

SATOYUKI TANAKA · HIROSHI OKADA · SHIGENOBU OKAZAWA

Received: date / Accepted: date

Abstract This study develops a wavelet Galerkin method (WGM) that uses B-spline wavelet bases for application to solid mechanics problems. A fictitious domain is often adopted to treat general boundaries in WGMs. In the analysis, the body is extended to its exterior but very low stiffness is applied to the exterior region. The stiffness matrix in the WGM becomes singular without the use of a fictitious domain. The problem arises from the lack of linear independence of the basis functions. A technique to remove basis functions that can be represented by the superposition of the other basis functions is proposed. The basis functions are automatically eliminated in the pre conditioning step. An adaptive strategy is developed using the proposed technique. The solution is refined by superposing finer wavelet functions. Numerical examples of solid mechanics problems are presented to demonstrate the multiresolution properties of the WGM.

Keywords Finite Element Method · Wavelet Galerkin Method · B-spline Scaling/Wavelet Functions · Adaptive Analysis · Stress Concentration Problem

S. Tanaka, S. Okazawa
Graduate School of Engineering, Hiroshima University, 4-1,
Kagamiyama 1-chome, Higashi-Hiroshima,739-8527, Japan
Tel.: +81-82-424-7859
Fax: +81-82-422-8527
E-mail: satoyuki@hiroshima-u.ac.jp

S.Okazawa
E-mail: okazawa@hiroshima-u.ac.jp

H. Okada
Department of mechanical Engineering, Faculty of Science
and Technology, Tokyo University of Science, 2641 Yamazaki,
Noda, 278-8510, Japan
E-mail: hokada@rs.noda.tus.ac.jp

1 Introduction

Although large-scale computer simulations using the finite element method (FEM) have become useful with developments in computer hardware, there are problems in generating large-scale finite element (FE) meshes. Methodologies that eliminate the need for meshes or elements have been proposed and can be categorized as "meshless" and "virtually meshless" FEMs. The "meshless" FEMs are represented by the element-free Galerkin Method [1], the reproducing Kernel Particle Method [2], and the meshless local Petrov-Galerkin method [3]. Unlike conventional FEMs, they have no meshes or elements and they eliminate the need for element connectivity information as input data. The free-mesh method [4] and voxel FEM [5] are examples of "virtually meshless" FEMs. They also do not require element connectivity data as input, but they use elements in their computations. In this study, a new "virtually meshless" FE approach based on B-spline wavelet basis functions is presented.

In recent years, wavelet methods have become powerful mathematical tools for representing a signal or a function in science and engineering research [6] [7] [8] [9] [10]. In the wavelet methods, scaling/wavelet functions are used as basis functions. These basis functions have so-called multiresolution properties. It is relatively easy to control spatial and time resolutions using a scaling function and wavelet functions of different length scales. In recent years, it has been found that the wavelet Galerkin method (WGM) is an efficient tool for solving partial differential equations. The WGM uses the wavelet basis functions as the Galerkin basis functions. The method does not require "meshes" or "elements" and can thus be considered a "virtually meshless" meth-

ods.

The wavelet basis functions have the ability to represent a function at different resolution levels. The solution can be refined in regions of high gradient such as stress concentration, without remeshing the entire analysis domain. Some researches have attempted to solve boundary value problems using the WGM. The two-dimensional Poisson equation is solved using the WGM and incorporating Green's function [11]. Beam and plate bending problems have been solved using Daubechie's wavelet functions [12]. Large-scale boundary value problems on domains having simple geometry have been solved [13] and the method has been extended to problems of three-dimensional layout optimization [14]. Mindlin plates analyses have been performed using cubic B-spline scaling functions, and the locking-free property of the WGM has been demonstrated [15]. A spline wavelet finite-element is proposed for beam, two-dimensional and three-dimensional elements. The spline wavelet bases are used in the element formulation as the shape function. The element-based formulation can treat the boundary condition easily [16]. In addition, one-dimensional thin-walled box beam analyses have been carried out using hat interpolation wavelet basis functions [17].

In spite of the development of WGMs, there are problems in the treatment of general boundaries when physical values (e.g. displacements, stresses) are represented by the sum of scaling/wavelet functions with their coefficients directly. To overcome the problems, two popular techniques are used. One is the fictitious domain approach [13] [14] and the other is the boundary-corrected scaling/wavelet functions approach [18] [19]. In the fictitious domain approach, the body is extended to its exterior, but very small stiffness (Young's modulus) is given to the exterior region. When the fictitious domain approach is adopted with a penalty formulation to enforcing the displacement boundary condition, the stiffness matrix contains very large and very small elements. There is the possibility that the stiffness matrix will become ill conditioned, and the iterative equation solver may suffer from inadequate convergence. In the boundary-corrected wavelet basis functions approach, the ordinal basis functions are modified to fit the boundary geometry. One-dimensional elasto-plastic-damage analyses have been performed using boundary-corrected basis functions [18] [19]. However, there are difficulties in expanding the techniques to complex-shaped geometry in two-dimensional and three-dimensional boundary value problems. Although the fictitious domain is used in wavelet Galerkin analyses, boundary treatment approaches have been pro-

posed using hat interpolation wavelet basis functions without penalty parameters or Lagrange multipliers [20]. Furthermore, the methodology has been adopted for multiscale topology design optimization [21].

Pioneering work in the use of wavelet basis functions in meshfree particle methods is reported by Liu and Chen [22] and Li and Liu [23][24][25][26][27][28]. The relation between the wavelet method and reproducing kernel methods has been noted in the literature [22]. In addition, the method is based on the idea of "partition of unity" [29], and the hierarchical bases are constructed with wavelet-like functions in the framework of the reproducing kernel approximation [25] [26]. Two-dimensional and three-dimensional numerical simulations have been performed with hierarchical bases [27]. In the literature, the fundamental basis functions satisfy the so-called "partition of unity" and higher-order basis functions satisfy the so-called "partition of nullity". To construct linearly independent basis functions, some shape functions must be taken from the "partition of nullity". However, the wavelet functions used in this study do not have "partition of nullity". We examine the issue in detail in terms of the function locations and find that the problem arises from the lack of linear independence of the wavelet basis functions on the boundary of the body.

In this study, we propose an adaptive WGM for two-dimensional solid mechanics problems that does not require a fictitious domain. Linear, quadratic and cubic B-spline scaling/wavelet functions [30] are used as the basis functions. Although the B-spline scaling/wavelet functions do not satisfy the so-called orthogonality condition [6] [7] [8] [10] in wavelet theory, the approach is suitable for solving boundary value problems. The B-spline basis functions have an explicit function form and are easy to integrate and differentiate. It is necessary to consider the boundary treatment in the WGMs with the B-spline scaling/wavelet functions as well as the analyses of the other wavelet basis functions. We examine the issue in detail in terms of the function locations and find that the problem arises from the lack of linear independence of the wavelet basis functions. To overcome the problem, we propose a technique to remove B-spline basis functions that can be expressed as the linear superposition of the other basis functions in the preconditioning process. An adaptive strategy using the multiresolution properties of the wavelet bases is presented. To improve the solution, finer wavelet functions are added where the numerical error is large. The adaptive strategies and convergence studies are presented for two-dimensional solid mechanics problems in numerical

examples.

2 Wavelet Galerkin Method

2.1 Multiresolution properties

An important issue in wavelet theory is the multiresolution property of the wavelet basis functions [6] [7] [8] [10]. A scaling function and wavelet functions with different length scales are used as the basis functions. These wavelet basis functions have the so-called multiresolution properties. In this section, we give a brief description of the multiresolution property for one-dimensional scaling/wavelet functions. In wavelet theory, a scaling function $\phi(x)$ has the so-called two-scale relationship, given by:

$$\phi(x) = \sum_k p_k \phi(2x - k) \quad (x_a < x < x_b), \quad (1)$$

where x_a and x_b are the analysis boundary and x is an internal point between x_a and x_b . The wavelet function $\psi(x)$ also has a two-scale relationship, given by:

$$\psi(x) = \sum_k q_k \phi(2x - k) \quad (x_a < x < x_b). \quad (2)$$

In eqs.(1) and (2), the coefficients p_k and q_k ($k = \text{integers}$) are the so-called two-scale sequences. The two-scale sequences are defined as a set of scaling/wavelet functions [6]. In wavelet theory, a function of resolution level j (simply referred to as level j hereafter) is approximated by the sum of the level j scaling functions $\phi_{j,k}(x)$, as:

$$f_j(x) = \sum_k a_{j,k} \phi(2^j x - k) = \sum_k a_{j,k} \phi_{j,k}(x), \quad (3)$$

where $a_{j,k}$ are coefficients of the scaling functions. The scaling functions are periodically located along the x_1 direction. The level j means that the scaling functions are located at $2^{-j}k$ ($k \in 0, 1, 2, \dots, 2^{-j}$) for a unit domain. In a similar manner, a level j function $g_j(x)$ is approximated by the sum of the level j wavelet functions $\psi_{j,k}(x)$, with their coefficients $b_{j,k}$, given as

$$g_j(x) = \sum_k b_{j,k} \phi(2^j x - k) = \sum_k b_{j,k} \psi_{j,k}(x). \quad (4)$$

The level $j + 1$ function $f_{j+1}(x)$ is represented by the superposition of the level j function $f_j(x)$ and the level j function $g_j(x)$ in eq. (4):

$$f_{j+1}(x) = f_j(x) + g_j(x). \quad (5)$$

The two-scale relationship of the scaling/wavelet functions in eqs. (1) and (2) and the function property in

eq. (5) are used repeatedly, and we thus construct the hierarchical structure of the wavelet basis functions, as:

$$f_{j+1}(x) = \sum_k a_{j_0,k} \phi_{j_0,k}(x) + \sum_{i=j_0}^j \sum_k b_{i,k} \psi_{i,k}(x), \quad (6)$$

where $\phi_{j_0,k}(x)$, $a_{j_0,k}$ are scaling functions with coefficients at level j_0 , and $\psi_{i,k}(x)$, $b_{i,k}$ ($i = j_0, \dots, j$) are wavelet functions with coefficients are from level j_0 to level j . This is the so-called multiresolution property of the scaling/wavelet functions in wavelet theory. The idea of the multiresolution property can easily be expanded to two-dimensional and three-dimensional problems.

2.2 B-spline scaling/wavelet functions

Scaling/wavelet functions are adopted as the basis functions in the formulation of WGMs, and here we use B-spline scaling/wavelet functions [6]. The functions have a compact support property and simple forms. They are represented by piecewise polynomial equations that are easy to integrate and differentiate. Although the scaling/wavelet functions do not satisfy the orthogonality condition in wavelet theory, they can be used as the basis functions in the WGM. The $m - th$ -order B-spline scaling/wavelet functions are represented by piecewise $(m - 1) - th$ -order polynomial functions, and their derivatives up to $(m - 2) - th$ order are continuous. The one-dimensional $m - th$ -order B-spline scaling function can be written as a power series:

$$\phi^{(m)}(x) = \frac{1}{(m-1)!} \sum_{k=0}^m (-1)^k {}_m C_k (x-k)_+^{m-1} \quad (7)$$

$$x_+ = \max\{0, x\} \quad (8)$$

$$x_+^m = (x_+)^m, \quad (9)$$

where the function support is

$$\text{supp } \phi^{(m)} = [0, m]. \quad (10)$$

The two-scale sequence p_k ($k = 0, \dots, m$) of the B-spline scaling function is

$$p_k = \frac{1}{2^{m-1}} {}_m C_k, \quad (k = 0, \dots, m) \quad (11)$$

In a similar way, the B-spline wavelet $\psi(x)$ has a two-scale sequence q_k ($k = 0, \dots, 3m - 2$):

$$q_k = \frac{(-1)^k}{2^{m-1}} \sum_l {}_m C_l \phi^{(2m)}(k+1-l), \quad (k = 0, \dots, 3m-2). \quad (12)$$

The function support is

$$\text{supp } \psi^{(m)} = [0, 2m - 1]. \quad (13)$$

Linear ($m = 2$), quadratic ($m = 3$) and cubic ($m = 4$) B-spline scaling/wavelet functions are used as wavelet Galerkin basis functions. The function forms are shown in Figs. 1 (a), (b) and (c). The function supports of the level j scaling function $\phi_{j,k}(x)$ and wavelet function $\psi_{j,k}(x)$ halve as the level $j \rightarrow j + 1$.

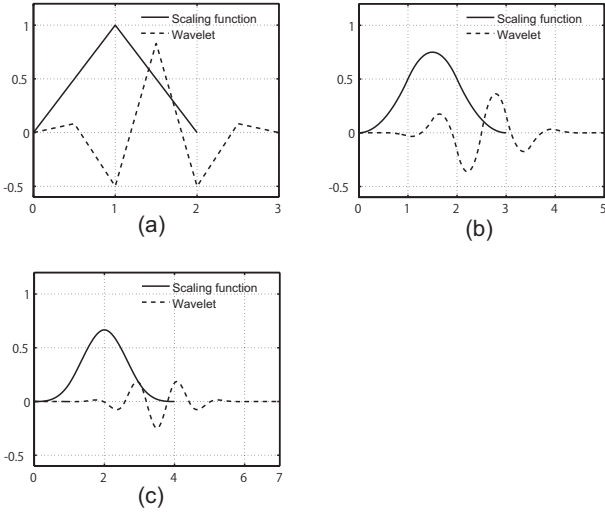


Fig. 1 One-dimensional m -th-order B-spline scaling/wavelet function [(a) Linear B-spline scaling/wavelet function ($m = 2$), (b) quadratic B-spline scaling/wavelet function ($m = 3$), (c) cubic B-spline scaling/wavelet function ($m = 4$)]

2.3 Wavelet Galerkin method using B-spline scaling/wavelet functions

In this section, we present the discretization of the WGM using the two-dimensional B-spline scaling/wavelet functions for elastostatic problems. A schematic illustration of the boundary value problem and the wavelet Galerkin discretization are shown in Figs. 2 (a) and (b). In Fig. 2 (a), the analysis domain is Ω and its boundary is Γ . The traction- and displacement-prescribed boundaries are Γ_t and Γ_u . In this method, the scaling functions are periodically located over the entire domain of analysis, and the wavelet functions are inserted locally where high spatial resolution is needed, such as at the edge of a hole as shown in Fig. 2 (b). Equally divided structured cells are placed in the analysis domain to integrate the stiffness matrices. The structured cells near the external boundary are equally divided as sub-cells to represent accurately the boundary of the body.

Numerical integration with Gauss quadrature is performed when the center of the sub-cell is located inside the boundary. The proposed method is thus considered a type of voxel approach [5].

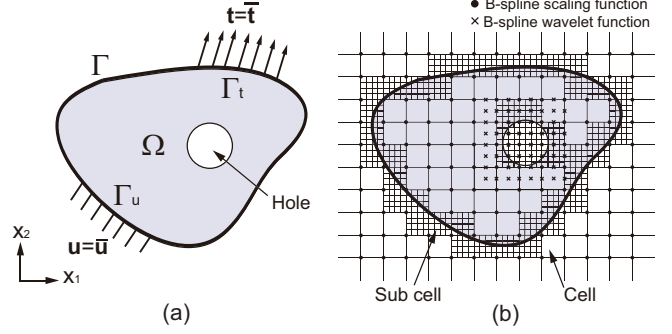


Fig. 2 B-spline wavelet Galerkin discretization [(a) Boundary value problem to be solved, (b) wavelet Galerkin discretization using B-spline scaling/wavelet function]

The boundary condition in Fig. 2 (a) is given by

$$\boldsymbol{\sigma}^T \cdot \mathbf{n} = \bar{\mathbf{t}} \quad \text{on } \Gamma_t, \quad (14)$$

$$\mathbf{u} = \bar{\mathbf{u}} \quad \text{on } \Gamma_u, \quad (15)$$

where $\boldsymbol{\sigma}$ is the stress tensor and \mathbf{n} is the normal of the boundary Γ . $\bar{\mathbf{t}}$ and $\bar{\mathbf{u}}$ are the prescribed traction and displacement on Γ_t and Γ_u , respectively. The B-spline scaling/wavelet functions do not have the so-called Kronecker delta property except for the linear B-spline scaling function. Thus, a penalty formulation is introduced to enforce the displacement boundary condition in eq. (15):

$$\int_{\Omega} \boldsymbol{\epsilon}(\delta \mathbf{u}) : \mathbf{D} : \boldsymbol{\epsilon}(\mathbf{u}) d\Omega - \int_{\Gamma_t} \delta \mathbf{u} \cdot \bar{\mathbf{t}} d\Gamma_t \quad (16)$$

$$+ \alpha \int_{\Gamma_u} \delta \mathbf{u} \cdot (\mathbf{u} - \bar{\mathbf{u}}) d\Gamma_u = 0,$$

where \mathbf{u} is the displacement and $\delta \mathbf{u}$ is its variation. $\boldsymbol{\epsilon}(\mathbf{u})$ and $\boldsymbol{\epsilon}(\delta \mathbf{u})$ are the symmetric parts of the displacement gradients and their variations. \mathbf{D} represents the elastic constants, and α is a penalty constant having a large positive value. In the WGM, the two-dimensional level $j + 2$ displacements $\mathbf{u}_{j+2}(x_1, x_2)$ are represented by the sum of the two-dimensional m -th-order level $j + 2$ B-spline scaling function $\Phi_{j+2,k,l}^{(m)}(x_1, x_2)$ ($k, l = \text{integers}$) with their coefficients $\mathbf{u}_{j+2,k,l}$:

$$\mathbf{u}_{j+2}(x_1, x_2) = \sum_k \sum_l \mathbf{u}_{j+2,k,l} \Phi_{j+2,k,l}^{(m)}(x_1, x_2) \quad (17)$$

These scaling functions are periodically located along the x_1 and x_2 directions. The scaling functions

$\Phi_{j+2,k,l}^{(m)}(x_1, x_2)$ are represented by the product of the one-dimensional scaling function $\phi_{j+2,k,l}^{(m)}(x_1)$ for the x_1 direction and $\phi_{j+2,k,l}^{(m)}(x_2)$ for the x_2 direction:

$$\Phi_{j+2,k,l}^{(m)}(x_1, x_2) = \phi_{j+2,k}^{(m)}(x_1)\phi_{j+2,k}^{(m)}(x_2). \quad (18)$$

The level $j+2$ displacement $\mathbf{u}_{j+2}(x_1, x_2)$ in eq. (17) can be rewritten using the multiresolution property of the B-spline scaling/wavelet functions:

$$\begin{aligned} \mathbf{u}_{j+2}(x_1, x_2) &= \sum_k \sum_l \mathbf{u}_{j,k,l} \Phi_{j,k,l}^{(m)}(x_1, x_2) \\ &+ \sum_{i=1}^3 \sum_k \sum_l \mathbf{v}_{j,k,l}^i \Psi_{j,k,l}^{i,(m)}(x_1, x_2) \\ &+ \sum_{i=4}^8 \sum_k \sum_l \mathbf{v}_{j+1,k,l}^i \Psi_{j+1,k,l}^{i,(m)}(x_1, x_2) \end{aligned} \quad (19)$$

where $\Phi_{j,k,l}^{(m)}(x_1, x_2)$, $\mathbf{u}_{j,k,l}$ are the level j scaling function and its coefficients. $\Psi_{j,k,l}^{i,(m)}(x_1, x_2)$, $\mathbf{v}_{j,k,l}^i$ ($i = 1, \dots, 3$) and $\Psi_{j+1,k,l}^{i,(m)}(x_1, x_2)$, $\mathbf{v}_{j+1,k,l}^i$ ($i = 4, \dots, 8$) are the level j and $j+1$ wavelet functions and their coefficients. The two-dimensional scaling/wavelet functions are represented by the product of the level j one-dimensional scaling functions and level j and $j+1$ wavelet functions. The scaling function is written as

$$\Phi_{j,k,l}^{(m)}(x_1, x_2) = \phi_{j,k}^{(m)}(x_1)\phi_{j,l}^{(m)}(x_2) \quad (20)$$

The wavelet functions are presented as

$$\begin{aligned} \Psi_{j,k,l}^{1,(m)}(x_1, x_2) &= \phi_{j,k}^{(m)}(x_1)\psi_{j,l}^{(m)}(x_2) \\ \Psi_{j,k,l}^{2,(m)}(x_1, x_2) &= \psi_{j,k}^{(m)}(x_1)\phi_{j,l}^{(m)}(x_2) \\ \Psi_{j,k,l}^{3,(m)}(x_1, x_2) &= \psi_{j,k}^{(m)}(x_1)\psi_{j,l}^{(m)}(x_2) \\ \Psi_{j+1,k,l}^{4,(m)}(x_1, x_2) &= \phi_{j,k}^{(m)}(x_1)\psi_{j+1,l}^{(m)}(x_2) \\ \Psi_{j+1,k,l}^{5,(m)}(x_1, x_2) &= \psi_{j,k}^{(m)}(x_1)\psi_{j+1,l}^{(m)}(x_2) \\ \Psi_{j+1,k,l}^{6,(m)}(x_1, x_2) &= \psi_{j+1,k}^{(m)}(x_1)\phi_{j,l}^{(m)}(x_2) \\ \Psi_{j+1,k,l}^{7,(m)}(x_1, x_2) &= \psi_{j+1,k}^{(m)}(x_1)\psi_{j,l}^{(m)}(x_2) \\ \Psi_{j+1,k,l}^{8,(m)}(x_1, x_2) &= \psi_{j+1,k}^{(m)}(x_1)\psi_{j+1,l}^{(m)}(x_2). \end{aligned} \quad (21)$$

In a similar manner, the higher-resolution displacements such as level $j+3$ displacements $\mathbf{u}_{j+3}(x_1, x_2)$ can be represented by adding the level $j+2$ wavelet functions $\Psi_{j+2,k,l}^{i,(m)}(x_1, x_2)$ ($i = 9, \dots, 15$) with their coefficients to the level $j+2$ displacements $\mathbf{u}_{j+2}(x_1, x_2)$ in eq. (17) or (19). Furthermore, the wavelet functions can be located where high spatial resolution is needed. Thus, it is easy to refine the numerical solution without employing remeshing procedures in the WGM. In matrix form, eqs. (17) and (19) can be rewritten as

$$\mathbf{u}_{j+2}(x_1, x_2) = \mathbf{N}_{j+2}(x_1, x_2) \cdot \mathbf{U}_{j+2}. \quad (22)$$

When the level $j+2$ scaling functions are used, the matrix $\mathbf{N}_{j+2}(x_1, x_2)$ and its coefficient vector \mathbf{U}_{j+2} are defined as

$$\mathbf{N}_{j+2}(x_1, x_2) = [\Phi_{j+2}], \quad (23)$$

$$\mathbf{U}_{j+2} = (\mathbf{u}_{j+2})^T, \quad (24)$$

When the level j scaling function and the level j and $j+1$ wavelet functions are used, the matrix $\mathbf{N}_{j+2}(x_1, x_2)$ and its coefficient vector \mathbf{U}_{j+2} are written, as

$$\mathbf{N}_{j+2}(x_1, x_2) = [\Phi_j \Psi_j^1 \cdots \Psi_j^3 \Psi_{j+1}^4 \cdots \Psi_{j+1}^8], \quad (25)$$

$$\mathbf{U}_{j+2} = (\mathbf{u}_j \mathbf{v}_j^1 \cdots \mathbf{v}_j^3 \mathbf{v}_{j+1}^4 \cdots \mathbf{v}_{j+1}^8)^T, \quad (26)$$

where \mathbf{u}_j , \mathbf{v}_j^i ($i = 1, 2, 3$), \mathbf{v}_{j+1}^i ($i = 4, \dots, 8$) correspond to vectors $\{\mathbf{u}_{j,k,l}\}$, $\{\mathbf{v}_{j,k,l}^i\}$, and $\{\mathbf{v}_{j+1,k,l}^i\}$, respectively. The matrices Φ_j , Ψ_j^i , and Ψ_{j+1}^i may be identified by equating eqs (17) and (19).

Here, we substitute the matrix form of eq. (22) into the penalty formation in eq. (16), and the linear simultaneous equation is obtained, as:

$$(\mathbf{K} + \mathbf{K}_\alpha)\mathbf{U}_{j+2} = \mathbf{f} + \mathbf{f}_\alpha \quad (27)$$

where \mathbf{U}_{j+2} is an unknown vector of level $j+2$ and \mathbf{K} is the global stiffness matrix. The unknown vector \mathbf{U}_{j+2} represents eq. (24) with a level $j+2$ scaling function, and eq. (26) with level j scaling/wavelet functions and a level $j+1$ scaling function. The stiffness matrix is described using eq. (26) as

$$\mathbf{K} = \begin{bmatrix} \mathbf{K}_{\Phi_j, \Phi_j} & \mathbf{K}_{\Phi_j, \Psi_j^1} & \cdots & \mathbf{K}_{\Phi_j, \Psi_j^3} & \mathbf{K}_{\Phi_j, \Psi_{j+1}^4} & \cdots & \mathbf{K}_{\Phi_j, \Psi_{j+1}^8} \\ & \mathbf{K}_{\Psi_j^1, \Psi_j^1} & \cdots & \mathbf{K}_{\Psi_j^1, \Psi_j^3} & \mathbf{K}_{\Psi_j^1, \Psi_{j+1}^4} & \cdots & \mathbf{K}_{\Psi_j^1, \Psi_{j+1}^8} \\ & & \ddots & & & & \\ & & & \mathbf{K}_{\Psi_j^3, \Psi_j^3} & \mathbf{K}_{\Psi_j^3, \Psi_{j+1}^4} & \cdots & \mathbf{K}_{\Psi_j^3, \Psi_{j+1}^8} \\ & sym & & & \mathbf{K}_{\Psi_{j+1}^4, \Psi_{j+1}^4} & \cdots & \mathbf{K}_{\Psi_{j+1}^4, \Psi_{j+1}^8} \\ & & & & & \ddots & \\ & & & & & & \mathbf{K}_{\Psi_{j+1}^8, \Psi_{j+1}^8} \end{bmatrix}. \quad (28)$$

When the level $j+2$ scaling functions in eq. (17) are used as the basis functions, the global stiffness matrix can be written as

$$\mathbf{K} = [\mathbf{K}_{\Phi_{j+2}, \Phi_{j+2}}], \quad (29)$$

The vector \mathbf{f} in eq. (27) is described as

$$\mathbf{f} = \int_{\Gamma_t} \mathbf{N}_{j+2}^T \cdot \bar{\mathbf{t}} d\Gamma_t, \quad (30)$$

where $\bar{\mathbf{t}}$ is a traction vector. \mathbf{K}_α and \mathbf{f}_α are the matrix and the vector of the penalty term to enforce the displacement boundary condition:

$$\mathbf{K}_\alpha = \int_{\Gamma_u} \mathbf{N}_{j+2}^T \cdot \mathbf{N}_{j+2} d\Gamma_u, \quad (31)$$

$$\mathbf{f}_\alpha = \int_{\Gamma_u} \mathbf{N}_{j+2}^T \cdot \bar{\mathbf{u}} d\Gamma_u, \quad (32)$$

where matrix \mathbf{N}_{j+2} is represented by eq. (23) for the analysis with level $j+2$ scaling functions, and by eq. (25) for the analysis with level j scaling/wavelet functions and level $j+1$ wavelet functions.

3 Treatment of the External Boundary

3.1 Treatment of the external boundary

In this section, we describe the treatment of the external boundary in the WGM with m -th-order B-spline scaling/wavelet functions. Analyses of a rectangular plate (Young's modulus E) under a tension load are carried out. A schematic illustration of the model is shown in Fig. 3 (a) and the boundary conditions are shown in Fig. 3 (b). Numerical integration of the stiffness matrix is performed using the periodically located structured cells. When the level $j+1$ scaling functions $\Phi_{j+1,k,l}^{(m)}(x_1, x_2)$ are adopted as the basis functions to represent level $j+1$ displacement $\mathbf{u}_{j+1}(x_1, x_2)$, the analysis can be performed without any difficulties. However, the global stiffness matrix is singular when the level j scaling functions $\Phi_{j,k,l}^{(m)}(x_1, x_2)$ and the wavelet functions $\Psi_{j,k,l}^{i,(m)}(x_1, x_2) (i = 1, 2, 3)$ are used as the basis functions to represent the level $j+1$ displacement $\mathbf{u}_{j+1}(x)$. We examine the problem in detail using the function locations and function supports, and find that the problem from a lack of linear independence of the basis functions.

One approach to overcome the above problem is to employ the so-called fictitious domain that is often used in the analysis of the WGM (e.g., [13][14]). A schematic illustration of the fictitious domain approach to the rectangular problem is shown in Fig. 3 (c). In the fictitious domain approach, a body is extended to its exterior but a very small stiffness $E^* (\ll E)$ is applied to the exterior region. Although level j B-spline scaling/wavelet functions are adopted as the basis functions, the analyses can be performed because the global stiffness matrix is not singular. However, the global stiffness matrix has very large and very small stiffness elements when the penalty formulation is adopted to enforce the displacement boundary condition. The iterative linear equation solver may suffer from convergence problems because the global stiffness matrix becomes ill conditioned. A similar problem arises for the boundary treatment in the analysis of the quadratic/cubic wavelet basis functions. To treat the boundary problem,

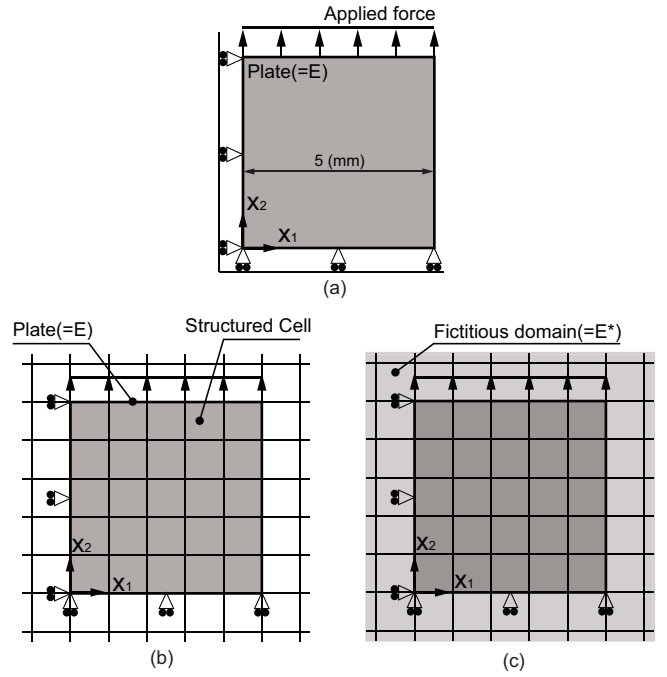


Fig. 3 Analysis of a square plate using the WGM with B-spline basis functions [(a) analysis for a rectangular plate, (b) analysis without a fictitious domain, (c) analysis with a fictitious domain]

we present an approach to eliminate any basis function that can be expressed by the linear superposition of the other wavelet basis functions.

3.2 A technique to remove basis functions

As mentioned above, the problem of the boundary treatment in the WGM is covered by the linear dependence of the wavelet basis functions. We propose a technique to remove basis functions that can be represented by the linear combination of the other basis functions. The function locations and the arrangement of the one-dimensional level j linear ($m = 2$) B-spline scaling/wavelet functions are shown in Fig. 4 (a). x_{boun} is the external boundary of the analysis domain and the numerical integration for the stiffness matrix is performed over $x_{boun} < x$. There are wavelet functions $\psi_{j,k-1}^{(2)}(x)$, $\psi_{j,k}^{(2)}(x)$ and $\psi_{j,k+1}^{(2)}(x)$ on the boundary x_{boun} . The integration regions of the wavelet functions $\psi_{j,k-1}^{(2)}(x)$ and $\psi_{j,k}^{(2)}(x)$ are less than half of the function supports, and the integration region of the wavelet function $\psi_{j,k+1}^{(2)}(x)$ is greater than half of the function support. In this case, the wavelet functions $\psi_{j,k-1}^{(2)}(x)$ and $\psi_{j,k}^{(2)}(x)$ can be represented by the superposition of the other scaling/wavelet functions. On the other hand, the wavelet function $\psi_{j,k+1}^{(2)}(x)$ is not represented by the superposition of the

other basis functions. We then remove degrees of freedom in terms of the wavelet functions $\psi_{j,k-1}^{(2)}(x)$ and $\psi_{j,k}^{(2)}(x)$ from the global stiffness matrix. The same approach can be expanded to the analysis of the quadratic, and cubic B-spline scaling/wavelet functions. Function locations and the arrangement of the quadratic ($m = 3$) B-spline bases are shown in Fig. 4 (b). The integration regions of the wavelet functions $\psi_{j,k-2}^{(3)}(x)$, $\psi_{j,k-1}^{(3)}(x)$ and $\psi_{j,k}^{(3)}(x)$ are less than half of their function supports, and the integration region of the wavelet function $\psi_{j,k+1}^{(3)}(x)$ is greater than half of the function support. In this case, we delete the degrees of freedom in terms of the wavelet functions $\psi_{j,k-2}^{(3)}(x)$, $\psi_{j,k-1}^{(3)}(x)$ and $\psi_{j,k}^{(3)}(x)$. In a similar manner, the case for the cubic ($m = 4$) B-spline scaling/wavelet functions is shown in Fig. 4 (c). The degrees of freedom correspond to the wavelet functions $\psi_{j,k-3}^{(4)}(x)$, $\psi_{j,k-2}^{(4)}(x)$, $\psi_{j,k-1}^{(4)}(x)$ and $\psi_{j,k}^{(4)}(x)$ for which the function supports are less than half of the function supports are removed.

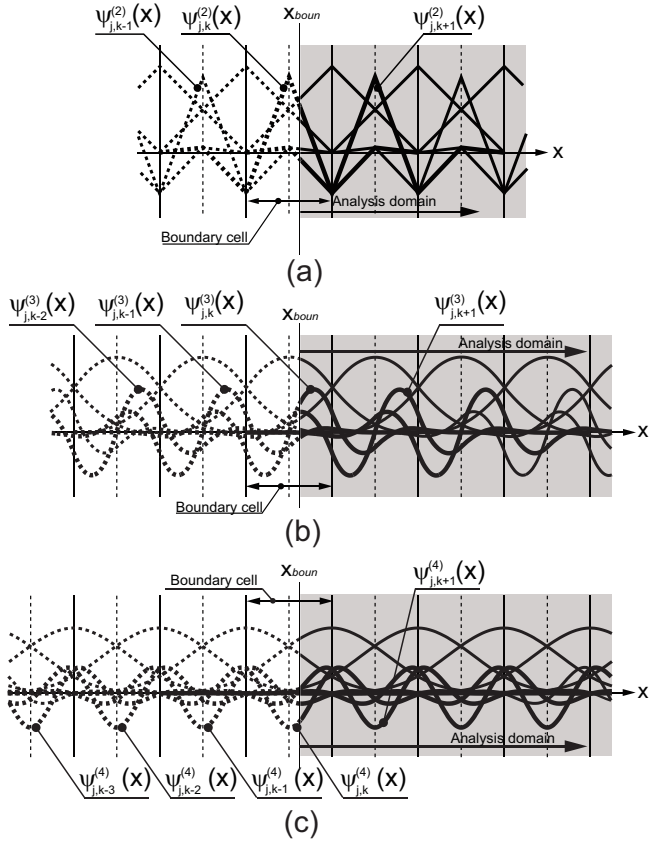


Fig. 4 Arrangement of B-spline scaling/wavelet function [(a) linear B-spline scaling/wavelet function, (b) quadratic B-spline scaling/wavelet function, (c) cubic B-spline scaling/wavelet function]

Typical cases of two-dimensional wavelet Galerkin discretization near the curved boundary are shown in Fig. 5(a) and (b). In these cases, a wavelet function is located on a hole in Fig. 5(a) and a wavelet function is located on two holes in Fig. 5(b). The discussion of the linear dependency is more complicated in the two-dimensional case. Here, we propose a technique to remove the wavelet functions in general problems as a pre-conditioning procedure.

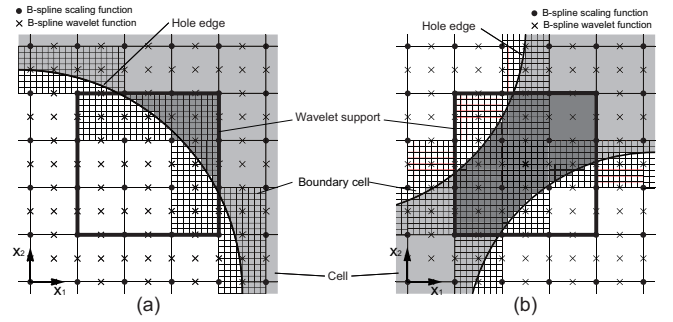


Fig. 5 Wavelet function near a hole edge [(a) wavelet function at a hole edge, (b) wavelet function at two hole edges]

In the WGM, eq. (27) is solved for unknown displacements. A unique solution exists only when the global stiffness matrix is not singular. When the global stiffness matrix suffers singular, a zero displacement field can be represented by a set of non-zero unknown vectors. We can examine the interpolation functions themselves instead of the stiffness matrix in eq. (27). To do so, we make use of scalar functions and the function with level $j + 2$ displacements in eq.(19) is represented by $u_{j+2}^P(\mathbf{x})$. The scalar function is written in matrix form as

$$u_{j+2}^P = [\mathbf{N}_{j+2}] \{ \mathbf{U}_{j+2}^P \}, \quad (33)$$

where \mathbf{N}_{j+2} is given by eq. (25) and \mathbf{U}_{j+2}^P is written as

$$\mathbf{U}_{j+2}^P(x_1, x_2) = \left(\mathbf{U}_j \mathbf{V}_j^{1,P} \dots \mathbf{V}_j^{3,P} \mathbf{V}_{j+1}^{4,P} \dots \mathbf{V}_{j+1}^{8,P} \right)^T, \quad (34)$$

where \mathbf{U}_j , $\mathbf{V}_j^{i,P}$, ($i = 1, \dots, 3$) and $\mathbf{V}_{j+1}^{i,P}$, ($i = 4, \dots, 8$) are parameter vectors of the level j scaling function and level j and $j + 1$ wavelet functions. When zero displacement is represented by eq. (19), the scalar function can be written as,

$$u_{j+2}^P = 0 \quad (35)$$

In addition, a function $J[u_{j+2}^P]$ is introduced according to the scalar function u_{j+2}^P :

$$J[u_{j+2}^P] = \int_{\Omega} \{ u_{j+2}^P(\mathbf{x}) \}^2 d\Omega \quad (36)$$

where Ω is the analysis domain. The function $J[u_{j+2}^P]$ is the domain integral value for the square of the scalar function $u_{j+2}^P(\mathbf{x})$, which has a positive value except for $u_{j+2}^P = 0$. According to eq. (33), the function $J[u_{j+2}^P]$ is represented in matrix form as

$$J[u_{j+2}^P] = \{\mathbf{U}_{j+2}^P\}^T [\mathbf{A}] \{\mathbf{U}_{j+2}^P\}, \quad (37)$$

the coefficient matrix $[\mathbf{A}]$ is written as

$$[\mathbf{A}] =$$

$$\int_{\Omega} \begin{bmatrix} \Phi_j^T \Phi_j & \Phi_j^T \Psi_j^1 & \dots & \Phi_j^T \Psi_j^3 & \Phi_j^T \Psi_{j+1}^4 & \dots & \Phi_j^T \Psi_{j+1}^8 \\ & \Psi_j^{1T} \Psi_j^1 & \dots & \Psi_j^{1T} \Psi_j^3 & \Psi_j^{1T} \Psi_{j+1}^4 & \dots & \Psi_j^{1T} \Psi_{j+1}^8 \\ & & \ddots & & & & \\ & & & \Psi_j^{3T} \Psi_j^3 & \Psi_j^{3T} \Psi_{j+1}^4 & \dots & \Psi_j^{3T} \Psi_{j+1}^8 \\ & & & & \Psi_{j+1}^{4T} \Psi_{j+1}^4 & \dots & \Psi_{j+1}^{4T} \Psi_{j+1}^8 \\ & & & & & \ddots & \\ & & & & & & \Psi_{j+1}^{8T} \Psi_{j+1}^8 \end{bmatrix} d\Omega. \quad (38)$$

In eq. (37), if $J[u_{j+2}^P] = 0$ for a non-zero coefficient vector ($\{\mathbf{U}_{j+2}^P\} \neq \{\mathbf{0}\}$), the matrix $[\mathbf{A}]$ is singular. Therefore, if $\{\mathbf{U}_{j+2}^P\} \neq \{\mathbf{0}\}$, then

$$[\mathbf{A}] \{\mathbf{U}_{j+2}^P\} = \{\mathbf{0}\}. \quad (39)$$

Vector \mathbf{U}_{j+2}^P that satisfies eq. (39) indicates the linear dependence of the values in eq. (33). By applying the fully pivoted Gauss-Jordan method [32] and appropriately reordering the right hand side vector of eq. (39), we obtain

$$\begin{bmatrix} \mathbf{I} & \tilde{\boldsymbol{\kappa}} \\ \mathbf{0} & \mathbf{0} \end{bmatrix} \begin{Bmatrix} \tilde{\mathbf{U}}_{j+2}^{P,I} \\ \tilde{\mathbf{U}}_{j+2}^{P,D} \end{Bmatrix} = \{\mathbf{0}\} \quad (40)$$

Here, \mathbf{I} and $\mathbf{0}$ are the identity and zero matrices. $\tilde{\mathbf{U}}_{j+2}^{P,D}$ is a vector of values that are expressed in terms of linear combinations of the basis functions of $\tilde{\mathbf{U}}_{j+2}^{P,I}$. $\tilde{\mathbf{U}}_{j+2}^{P,I}$ is the value of independent quantities of the level j scaling function and level j and $j+1$ wavelet functions. From eq. (40), we have

$$\{\tilde{\mathbf{U}}_{j+2}^{P,I}\} + [\tilde{\boldsymbol{\kappa}}] \{\tilde{\mathbf{U}}_{j+2}^{P,D}\} = \{\mathbf{0}\}. \quad (41)$$

It is clear that $\tilde{\mathbf{U}}_{j+2}^{P,D}$ and $\tilde{\mathbf{U}}_{j+2}^{P,I}$ are linearly dependent on each other. We adopted the same technique to check linear dependency in analysis employing mesh superposition technique (s-FEM)[33].

When applying the fully pivoted Gauss-Jordan method to the coefficient matrix in eq. (39), the diagonals with respect to nodal degrees of freedoms that are not linearly independent become zeros, as stated in eq.

(40). However, although the diagonal terms should become zeros, they tend to very small numbers. Therefore, we write

$$\begin{bmatrix} \mathbf{I} & \tilde{\boldsymbol{\kappa}} \\ \mathbf{0} & \mathbf{p} \end{bmatrix} \begin{Bmatrix} \tilde{\mathbf{U}}_{j+2}^{P,I} \\ \tilde{\mathbf{U}}_{j+2}^{P,D} \end{Bmatrix} = \{\mathbf{0}\}, \quad (42)$$

where \mathbf{p} is a matrix whose elements are very small. Thus, we introduce a threshold value ϵ to judge a zero value. If the diagonal terms of matrix \mathbf{p} are smaller than the threshold value ϵ ($< 10^{-5}$), the associated nodal quantities are judged to be linearly dependent. The degrees of freedom associated with those nodes are then eliminated.

When essential boundary conditions are enforced in regions of the deleted wavelet functions, penalty formulation presented in chapter 2.3 can also be adopted. The new matrix $\mathbf{N}'_{j+2}(x_1, x_2)$ and its coefficients \mathbf{U}'_{j+2} are constructed by a set of linear independent scaling/wavelet functions in the same as eqs. (25) and (26). The matrix $\mathbf{N}'_{j+2}(x_1, x_2)$ and the vectors \mathbf{U}'_{j+2} are substituted in penalty terms in eqs. (31) and (32).

In the WGM, the $m - th$ -order B-spline scaling function and wavelet functions of different length scales are used as the basis functions. Among the multiresolution properties, the scaling function represents global displacement and the wavelet functions represent local displacements. We then let the components of $\tilde{\mathbf{U}}_{j+2}^{P,D}$ include the wavelet functions only, so that we can remove the freedoms associated with the wavelet functions. To solve eq. (39) employing the fully pivoted Gauss-Jordan method, elimination first is carried out in terms of degrees of freedom of the scaling function. We then remove unnecessary freedoms associated with the wavelet basis functions.

4 Numerical Examples

The previous section presented the treatment of the external boundary in the WGM using B-spline scaling/wavelet functions. The problem relates to the linear independence of the wavelet basis functions. We proposed a technique to remove wavelet basis functions in the pre-conditioning process. To verify the proposed approach, we presented the two-dimensional solid mechanics problems.

4.1 Multiresolution properties

Analyses are performed for a rectangular plate with a hole. The model and boundary condition are shown in

Fig. 6 (a). The WGM model is shown in Fig. 6 (b). The plate is divided into 10×10 equallare divided into 128×128 equally spaced sub-cells and the numerical integrations for the stiffness matrices are performed when the center of the sub-cell is located inside the analysis domain. The level j scaling function $\Phi_j^{(m)}(x_1, x_2)$, level j wavelet function $\Phi_j^{i,(m)}(x_1, x_2)$ ($i = 1, 2, 3$) and level $j + 1$ wavelet function $\Phi_{j+1}^{i,(m)}(x_1, x_2)$ ($i = 4, \dots, 8$) are used as the basis functions to represent the level $j + 2$ displacement $\mathbf{u}_{j+2}(x_1, x_2)$. In this example, the problem of linear dependence occurs near the hole edge. The wavelet basis functions are checked in the preconditioning process, and particular wavelet functions are removed.

To confirm the multiresolution properties of the wavelet basis functions, the rectangular plate is divided into a 40×40 equally spaced structured cells and a level $j + 2$ scaling function $\Phi_j^{(m)}(x_1, x_2)$ is applied. The analysis model is shown in Fig. 6 (c). The boundary cells are divided into 32×32 sub-cells so as to coincide with the boundary geometry of Fig. 6 (b). The numerical results for the analyses with linear, quadratic and cubic B-spline basis functions are shown in Figs. 7 (a), (b) and (c). The variations in normalized stress σ_{22}/σ along the bottom edge of the plate are shown. In all cases, the same values are obtained with the level j scaling function plus level $j, j + 1$ wavelet functions, and with the level $j + 2$ scaling functions. From the numerical results, the multiresolution properties of the WGM are confirmed, and it is recognized that the proposed techniques are effective in the analysis of the WGM with B-spline basis functions. It is also noted that application of a fictitious domain is not necessary.

4.2 Rectangular plate with two holes

A more complicated problem is solved with the proposed technique. Two holes are located on a $10\text{mm} \times 10\text{mm}$ rectangular plate. The analysis model is shown in Fig. 8(a). The problem of linear dependence of the basis function occurs near the hole edge. The WGM model is shown in Fig. 8(b). The rectangular plate is divided into 16×16 structured cells. The boundary cell that is located on the hole edge is divided into 128×128 sub-cells. In this analysis, a level j scaling function and level $j, j + 1$ wavelet functions are used to represent the level $j + 2$ displacements. Linear, quadratic and cubic B-spline bases are adopted respectively. The locations of basis functions are represented in Fig. 9 (a), (b) and (c). The filled (black color) and open circles (white color) represent the centers of the wavelet basis functions. The

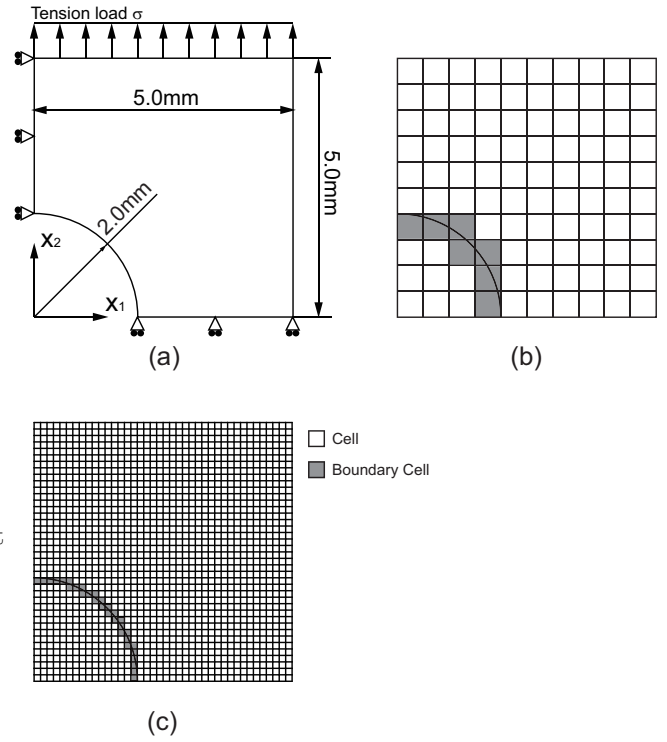


Fig. 6 A hole problem [(a) analysis model, (b) wavelet Galerkin model (10×10 division), (c) wavelet Galerkin model (40×40 division)]

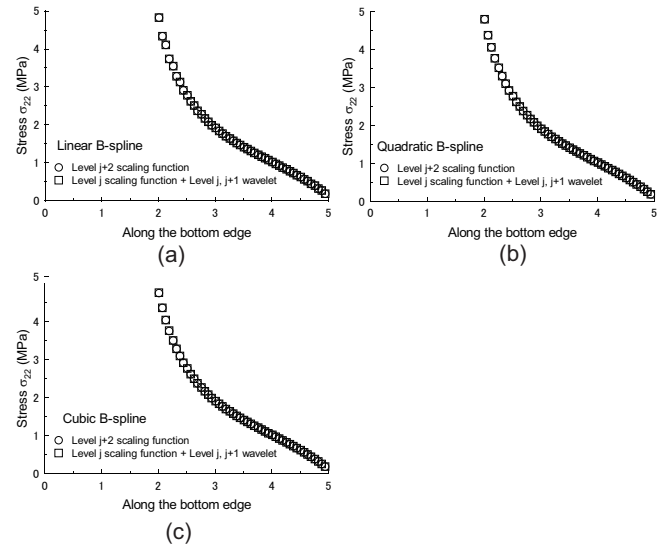


Fig. 7 Multiresolution analysis [(a) linear B-spline, (b) quadratic B-spline, (c) cubic B-spline]

basis functions that are not within in the hole in Fig. 9 (a), (b) and (c) are not used in the calculation of the stiffness matrix. In addition, the nodes deleted in the pre conditioning process are represented by the open circles. The basis functions of indicated by filled circles can construct linearly independent basis functions without employing a fictitious domain. Therefore, em-

employing the proposed technique, we can represent linearly independent basis functions for complex-shaped geometry.

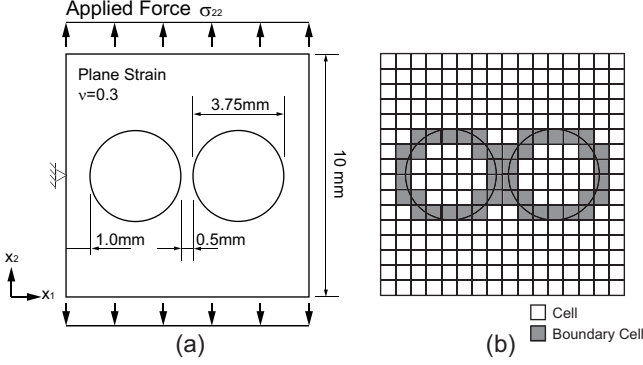


Fig. 8 Rectangular plate with two holes ($D = 3.75$ mm) [(a) analysis model, (b) wavelet Galerkin model]

4.3 Adaptive Analysis

A schematic illustration of the adaptive procedures using the WGM is shown in Fig. 10 (a). The locations of function with linear and cubic B-splines are shown in Fig. 10 (b), and that with a quadratic B-spline is shown in Fig. 10 (c). The points in the figures represent the centers of the basis functions. Although the function location of the quadratic B-spline is slightly different from the locations of the linear and cubic B-splines, the same adaptive approach can be applied. In this analysis, the lowest resolution level is assumed to be level j analysis.

In the first stage, the analyses are independently performed at two different levels (level j analysis, level $j + 1$ analysis) as shown in Fig. 10 (a). The function locations are presented in Figs. 10 (b) and (c). The square region surrounding four nodes represents a structured cell. An error estimation based on the energy error norm is adopted to refine the solution. The error estimator η_i ($i = \text{integers}$) is defined by each structured cell. The error estimation for the i -th cell is represented as,

$$\eta_i = \frac{\|\mathbf{E}_{j+1}\|_i}{\|\mathbf{U}_{j+1}\|_i} \times 100\%, \quad (43)$$

where $\|\mathbf{E}_{j+1}\|_i$ is the energy norm error for the i -th cell and $\|\mathbf{U}_{j+1}\|_i$ is the energy norm for the i -th cell. They are written as

$$\|\mathbf{E}_{j+1}\|_i = \left[\int_{\Omega_i} (\boldsymbol{\epsilon}^{j+1} - \boldsymbol{\epsilon}^j)^T (\boldsymbol{\sigma}^{j+1} - \boldsymbol{\sigma}^j) d\Omega_i \right]^{\frac{1}{2}}, \quad (44)$$

$$\|\mathbf{U}_{j+1}\|_i = \left[\int_{\Omega_i} (\boldsymbol{\epsilon}^{j+1})^T (\boldsymbol{\sigma}^{j+1}) d\Omega_i \right]^{\frac{1}{2}}, \quad (45)$$

where $\boldsymbol{\epsilon}^{j+1}$ and $\boldsymbol{\epsilon}^j$ are strain components and $\boldsymbol{\sigma}^{j+1}$ and $\boldsymbol{\sigma}^j$ are stress components for level j and $j + 1$ analysis. Ω_i is the domain size of the i -th cell. If the error estimator η_i is greater than a threshold $\bar{\eta}$, then the numerical solutions are locally refined by adding higher resolution wavelet functions according to the error estimation as shown in Figs. 10 (b) and (c). The structured cell is divided into four structured cells in a refinement process. The adaptive refinements are repeatedly performed until the numerical solution converges.

In some cases, there are regions where the energy norm $\|\mathbf{U}_{j+1}\|_i$ becomes very small, such as the neutral axis region of the beam under bending loads. In these regions, the error estimator η_i can no longer be accurately evaluated. In this case, the average energy norm $\|\mathbf{U}_{j+1}\|_{ave}$ is introduced to evaluate the error estimator

$$\|\mathbf{U}_{j+1}\|_{ave} = \frac{A_{cell}^{j+1}(i)}{A_{all}^{j+1}} \times \sqrt{\sum_{i=1}^{n_{j+1}} \|\mathbf{U}_{j+1}\|_i^2}, \quad (46)$$

where $A_{cell}^{j+1}(i)$ is the area of the i -th cell and A_{all}^{j+1} is the total area of the analysis domain in the level $j + 1$ analysis. n_{j+1} is the total number of cells in the level $j + 1$ analysis. If the energy norms $\|\mathbf{U}_{j+1}\|_i$ ($i = \text{integers}$) are less than the average norm $\|\mathbf{U}_{j+1}\|_{ave}$, we substitute $\|\mathbf{U}_{j+1}\|_{ave}$ with $\|\mathbf{U}_{j+1}\|_i$ in eq. (43). The error estimator η_i of the WGM with linear B-spline is larger than that of the analyses with the quadratic and cubic B-splines. The threshold $\bar{\eta}$ is assumed as $\bar{\eta} = 2.0\%$ for analysis with the linear B-spline and $\bar{\eta} = 1.0\%$ for analysis with quadratic and cubic B-splines. Relative error η' is also evaluated to check the convergence of the analysis in each refinement step. The relative error is evaluated in the entire analysis domain Ω as the same as the error estimation in eq. (43).

Employing the adaptive procedures, the problem of the rectangular plate with two holes is solved. The analysis model is shown in Fig.11 (a). The hole diameter is 1.5 mm. The wavelet Galerkin model is shown in Fig.11 (b). The rectangular plate is modeled with 16×16 equally spaced structured cells. The boundary cell is divided into 128×128 sub-cells to represent the hole geometry. The adaptive refinements are performed with linear, quadratic and cubic B-spline bases. The normalized stress distribution along the x direction of σ_{22}/σ with linear B-splines is presented in Fig. 12(a).

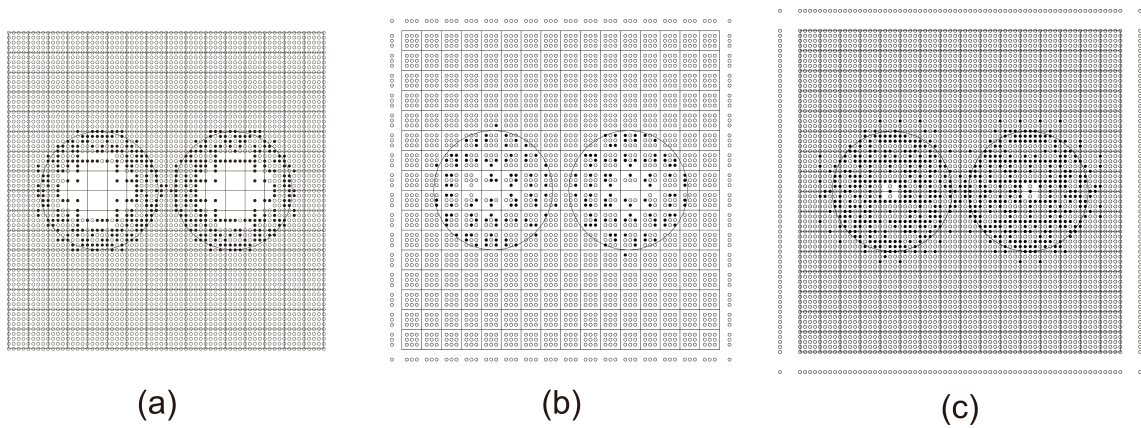


Fig. 9 Distribution of basis functions [(a) linear bases, (b) quadratic bases, (c) cubic bases]

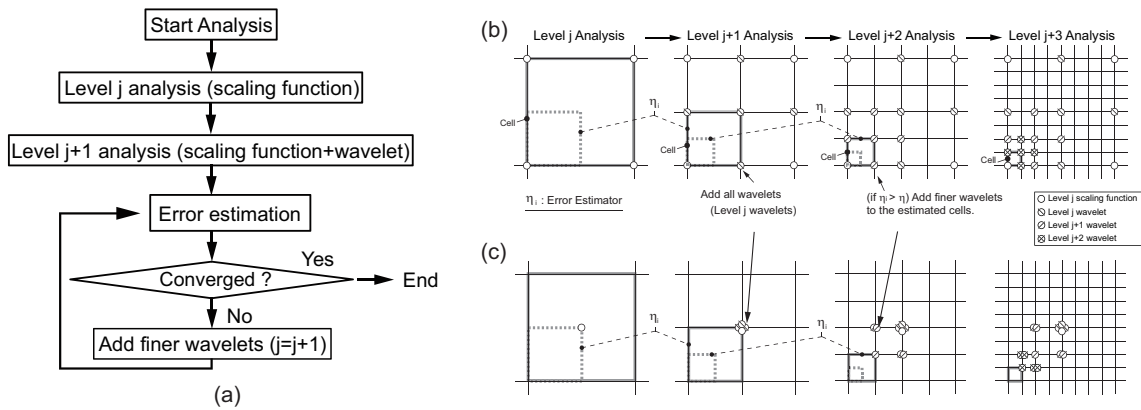


Fig. 10 Adaptive analysis [(a) flow chart of adaptive procedures, (b) function locations (linear B-spline, cubic B-spline), (c) function locations (quadratic B-spline)]

As a comparison, the result of FE analysis using MSC.Nastran is shown in the figure. As the refinements proceed, the numerical solution converges to the reference solution. In addition, the convergence of relative error η' is shown in Fig.12(b). The relative error η' is the sum of energy norm error in eq. (43). The solid lines represent the uniform refinement solution (without an adaptive procedure). In this figure, all adaptive analyses exhibit good convergence in all adaptive analyses. Especially, the convergence is enhanced when quadratic and cubic B-spline bases are used. The distribution of the wavelet basis functions is shown in Figs. 13(a), (b) and (c). As the refinement proceeds, the density of the basis functions increases near the region of stress concentration region. The trends are the same for all adaptive analyses.

Adaptive analysis is performed for a cantilever beam bending problem is performed. The analysis model is shown in Fig. 14 (a). The cantilever beam has four holes along the neutral axes. Shear stress is enforced on the right hand side of the beam and a fixed displacement

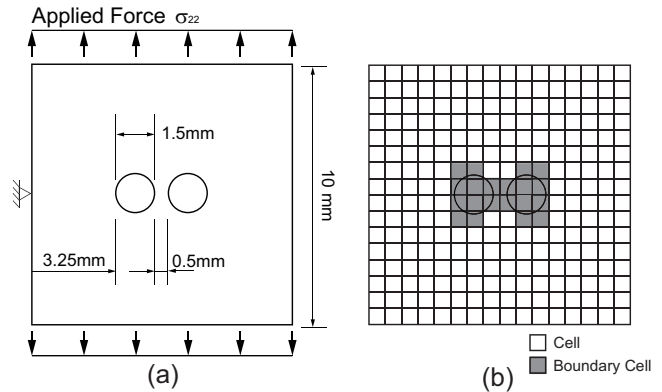


Fig. 11 Rectangular plate with two holes ($D = 1.5$ mm)[(a) Analysis model, (b) wavelet Galerkin model]

boundary condition is enforced on opposite side. The rectangular domain is divided into 12×24 equally spaced structured cells for the lowest-resolution (level j) analysis. Quadratic and cubic B-spline wavelet bases are used in the adaptive analysis. The function locations of the adaptive analyses are shown in Fig. 15 (a) with quadratic bases and Fig. 15 (b) with cubic bases.

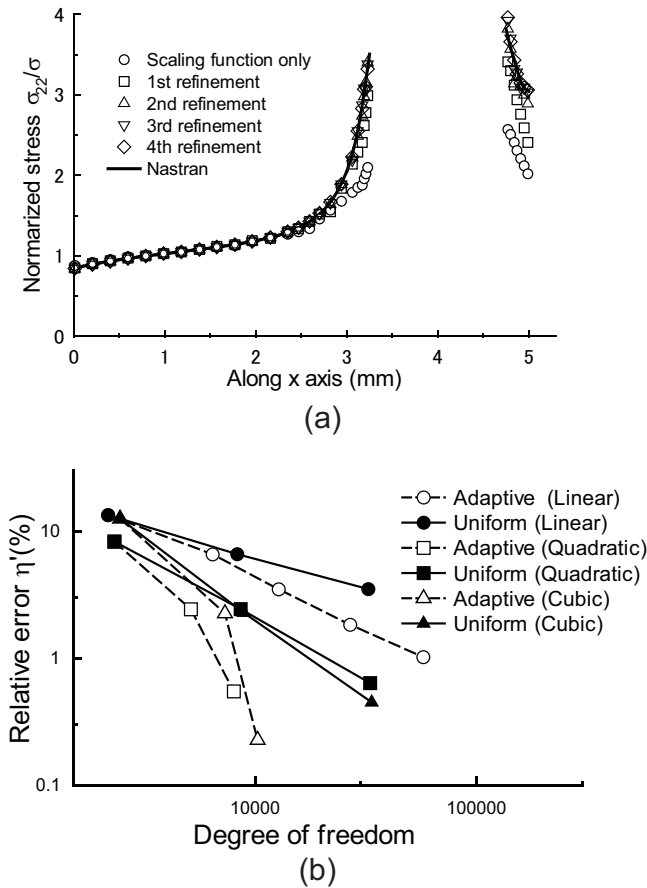


Fig. 12 Two hole problem [(a) refinements the solution σ_{zz} (linear B-spline), (b) relative energy norm error η']

As the adaptive analysis proceeds, the higher-order basis functions are located near the hole. The global error η' is presented in Fig. 17 (a). For comparison, uniform refinement results are shown in the figure. The numerical results show that the wavelet Galerkin analysis performs effectively in adopting the adaptive procedures. The use of cubic B-splines provides better convergence than the use of quadratic B-splines.

Adaptive analyses for a rectangular plate with randomly distributed holes are presented. The analysis model is shown in Fig. 14 (b). Uniform tension is applied to the plate. The rectangular domain is divided into 24×24 equally spaced structured cells for the lowest-resolution (level j) analysis. The adaptive analysis is performed with quadratic and cubic B-splines. The distributions of the basis functions are presented in Fig. 16 (a) for quadratic B-splines, and 16 (b) for cubic B-splines. The convergence is shown in Fig. 17 (b). Although the convergence is better in both cases than in the case of uniform refinement iterations, the convergence rate of the relative errors decreased in the final step when using cubic B-splines. The function supports

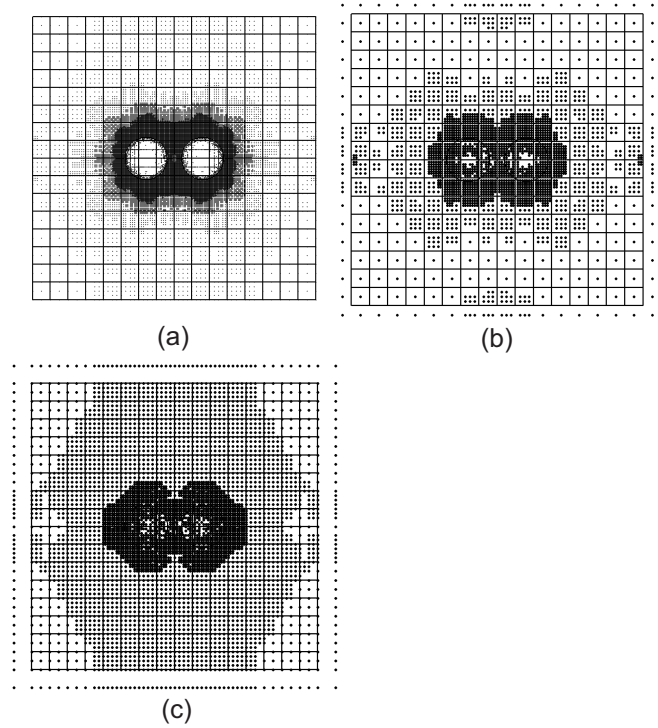


Fig. 13 Distribution of basis functions [(a) linear bases, (b) quadratic bases, (c) cubic bases]

of the low resolution basis functions of cubic B-splines are wider than those of the higher-resolution basis function. When there are high and low gradients in the support area of the low-resolution wavelet, the function cannot represent all the gradients at the same time. This is the reason why the convergence rate decreased. Following observation, another error estimator or adaptive strategy will be developed to evaluate a more severe stress concentration problem such as a notch or crack problem.

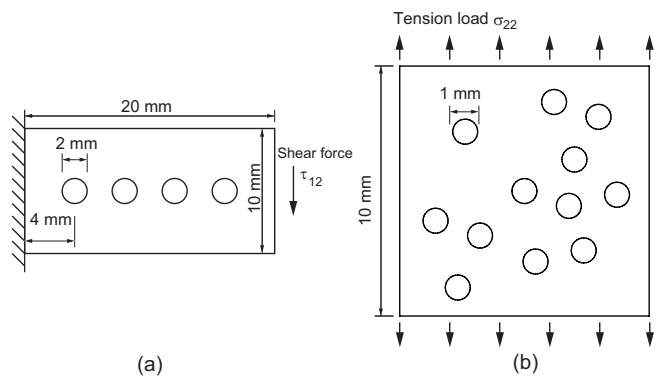


Fig. 14 Analysis model to be solved [(a) cantilever beam bending problem, (b) rectangular plate with randomly distributed holes]

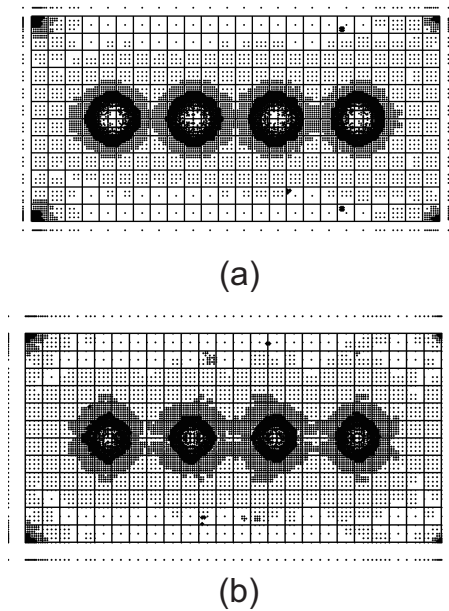


Fig. 15 Distribution of basis functions (cantilever beam bending problem) [(a) analysis with quadratic B-spline, (b) analysis with cubic B-spline]

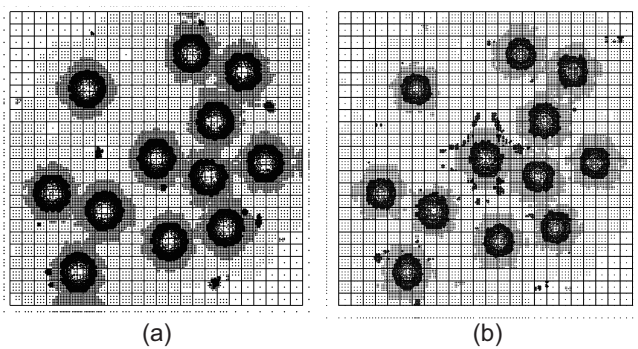


Fig. 16 Distribution of basis functions (rectangular plate with randomly-distributed holes) [(a) analysis with quadratic B-spline, (b) analysis with cubic B-spline]

5 Conclusion

We proposed an adaptive WGM for two-dimensional solid mechanics problems without the use of a fictitious domain. Linear, quadratic and cubic B-spline scaling/wavelet functions are used as the basis functions. In the WGM analysis, the stiffness matrix became singular because of the lack of linear independence of the basis functions when the fictitious domain is not used. To overcome this problem, we proposed a technique to remove B-spline basis functions that can be expressed by the linear superposition of the other basis functions in a pre conditioning step. An adaptive strategy with employing the WGM is presented and a refinement procedure is demonstrated. Adaptive analyses for two-dimensional

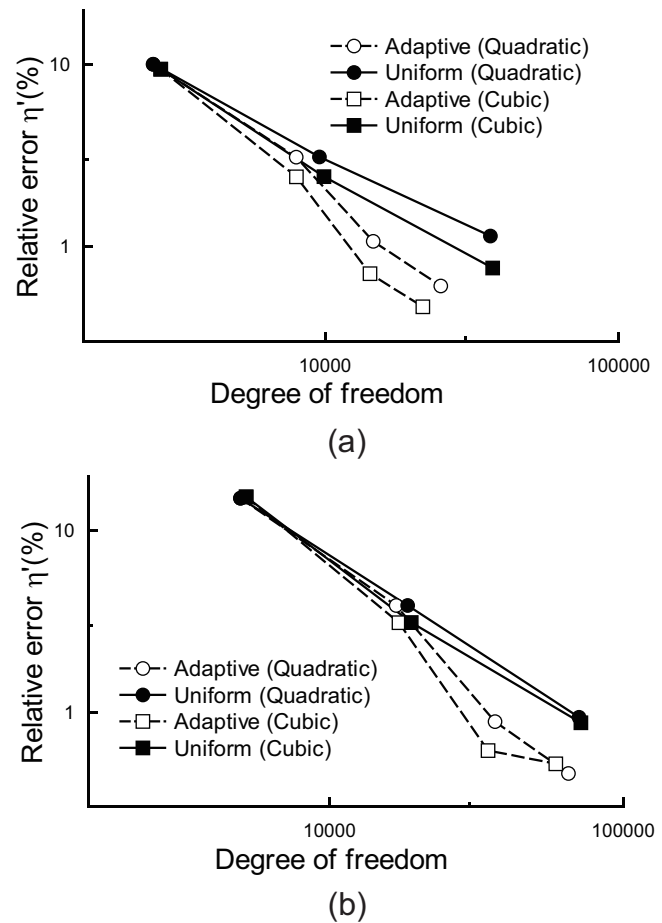


Fig. 17 Relative energy norm error η' [(a) cantilever beam bending problem, (b) rectangular plate with randomly-distributed holes]

solid mechanics problems are presented as numerical examples to confirm the problem.

References

1. Belytschko T., Lu Y. Y., Gu L., 1994, Element-free Galerkin Methods, *International Journal for Numerical Methods in Engineering*, 37, pp. 229-256.
2. Liu W. K., Jun S., Li S., Adee J., Belytschko T., 1995, Reproducing kernel particle methods for structural dynamics, *International Journal for Numerical Methods in Engineering*, 38, pp. 1655-1679.
3. Atluri S. N., Zhu T., 1998, A new meshless local Petrov-Galerkin (MLPG) approach in computational mechanics, *Computational Mechanics*, 22, pp. 117-127.
4. Yagawa G., Furukawa T., 2000, Recent developments of free mesh method, *International Journal for Numerical Methods in Engineering*, 47, pp. 1419-1443.
5. Hollister S. J., Kikuchi N., 1994, Homonization theory and digital imaging: A basis for studying the mechanics and design principles of bone tissue, *Biotechnology and Bioengineering*, 43, pp. 586-596.
6. Chui C. K., 1992, *An introduction to wavelets*, Academic Press.

7. Daubechies I., 1992, *Ten Lectures on Wavelets*, SIAM, Philadelphia.
8. Mayer Y. 1993, *Wavelets: Algorithms and Applications*, SIAM, Philadelphia.
9. Williams J. R., Amaratunga K., 1994, Introduction to wavelets in engineering, *International Journal for Numerical Methods in Engineering*, 37, pp. 2365-2388.
10. Chui C. K., 1997, *Wavelets: A Mathematical Tool for Signal Analysis*, SIAM, Philadelphia.
11. Amaratunga K. Williams J. R., Qian S., John W., 1994, Wavelet-Galerkin solutions for one dimensional partial differential equations, *International Journal for Numerical Methods in Engineering*, 27, pp. 2703-2716.
12. Youhe Z., Jizeng W. and Xiaojing, Z., 1998, Applications of wavelet Galerkin FEM to bending of beam and plate structures, *Applied Mathematics and Mechanics*, English Edition, 19, pp. 745-755.
13. Diaz A. R., 1999, A wavelet-Galerkin schemes for analysis of large-scale analysis on simple domains, *International Journal for Numerical Methods in Engineering*, 44, pp. 1599-1616.
14. DeRose Jr. C. G. A., Diaz A. R., 2000, Solving three-dimensional layout optimization problems using fixed scale wavelets, *Computational Mechanics*, 25, pp. 274-285.
15. Nakagoshi S., Noguchi H., 2001, A modified wavelet Galerkin method for analysis of mindlin plates, *JSME International Journal. Ser. A*, 44, pp. 610-615.
16. Han J. G., Ren W. X., Huang Y., A spline wavelet finite-element method in structural mechanics, *International Journal for Numerical Methods in Engineering*, 66, pp. 166-190.
17. Kim Y. Y., Jang G. W., 2002, Hat interpolation wavelet-based multi-scale Galerkin method for thin-walled box beam analysis, *International Journal for Numerical Methods in Engineering*, 53, pp. 1575-1592.
18. Venini P., Morana P., 2001, An adaptive wavelet-Galerkin method for an elastic-plastic-damage constitutive model: 1D problem, *Computer Methods in Applied Mechanics and Engineering*, 190, pp. 5619-5638.
19. Cominciol V., Scapolla T., Naldi G., Venini P. 2000, A wavelet-like Galerkin method for numerical solution of variational inequalities arising in elastoplasticity, *Communications in Numerical Methods in Engineering*, 16, pp. 133-144.
20. Jang G. W., Kim J. E., Kim Y. Y., 2004, Multiscale Galerkin method using interpolations wavelets for two-dimensional elliptic problems in general domains. *International Journal for Numerical Methods in Engineering*, 59, pp. 225-253.
21. Kim J. E., Jang G. W., Kim Y. Y., 2003, Adaptive multiscale wavelet-Galerkin analysis for plane elasticity problems and its application to multiscale topology design optimization, *International Journal of Solids and Structures*, 40, pp. 6473-6496.
22. Liu W. K, Chen Y., 1995, Wavelet and multiple scale reproducing kernel method. *International Journal for Numerical Methods in Fluids*, 21, pp.901-933.
23. Li S., Liu W. K., 1996, Moving least-square reproducing kernel method Part II: Fourier analysis, *Computer Methods in Applied Mechanics and Engineering*, 139, pp. 159-193.
24. Li S., Liu W. K., 1998, Synchronized reproducing kernel interpolant via multiple wavelet expansion, *Computational Mechanics*, 28, pp.28-47.
25. Li S., Liu W. K., 1999, Reproducing Kernel Hierarchical Partition of Unity, Part I - Formulation and Theory, *International Journal for Numerical Methods in Engineering*, 45, pp. 251-288.
26. Li S., Liu W. K., 1999, Reproducing Kernel Hierarchical Partition of Unity, Part II - Applications, *International Journal for Numerical Methods in Engineering*, 45, pp. 289-317.
27. Li S., Liu W. K., 2000, Numerical simulations of strain localization in inelastic solids using mesh-free methods, *International Journal for Numerical Methods in Engineering*, 48, pp. 1285-1309.
28. Li S., Liu W. K., 2004, *Meshfree Particle Methods*, Springer.
29. Melenk J. M., Babuška I., 1996, The partition of unity finite element method: basic theory and applications., *Computer Methods in Applied Mechanics and Engineering*, 139, pp. 289-314.
30. Chui C. K., Wang G. Z., 1991, A cardinal spline approach to wavelet, *Proceeding of the American Mathematical Society*, 113, pp. 785-793.
31. Zienkiewicz O. C, Taylor R. L., 2000, *The finite element method*, Volume 1, The basis, Butterworth heinemann.
32. Press W. H., Teukolsky S. A., Vettering W. T., Flannery B. P., 1992, *Numerical Recipes in Fortran 77 in 2nd Ed.*, Cambridge University Press.
33. Ooya T., Tanaka S., Okada H., 2009, On the Linear Dependencies of Interpolation Functions in s-Version Finite Element Method, *Journal of Computational Science and Technology*, 3, pp. 124-135.